ATLAS Internal Note
INDET-NO-066
17 October 1994

Inner Detector Layout for Technical Proposal

J. Baines, A. Dellacqua, F. Fares, D. Froidevaux and P. Nevski

Abstract

This note summarises the main features of the ATLAS inner detector, as they have been agreed upon for the Technical Proposal during the September ATLAS week.

1 Overall features

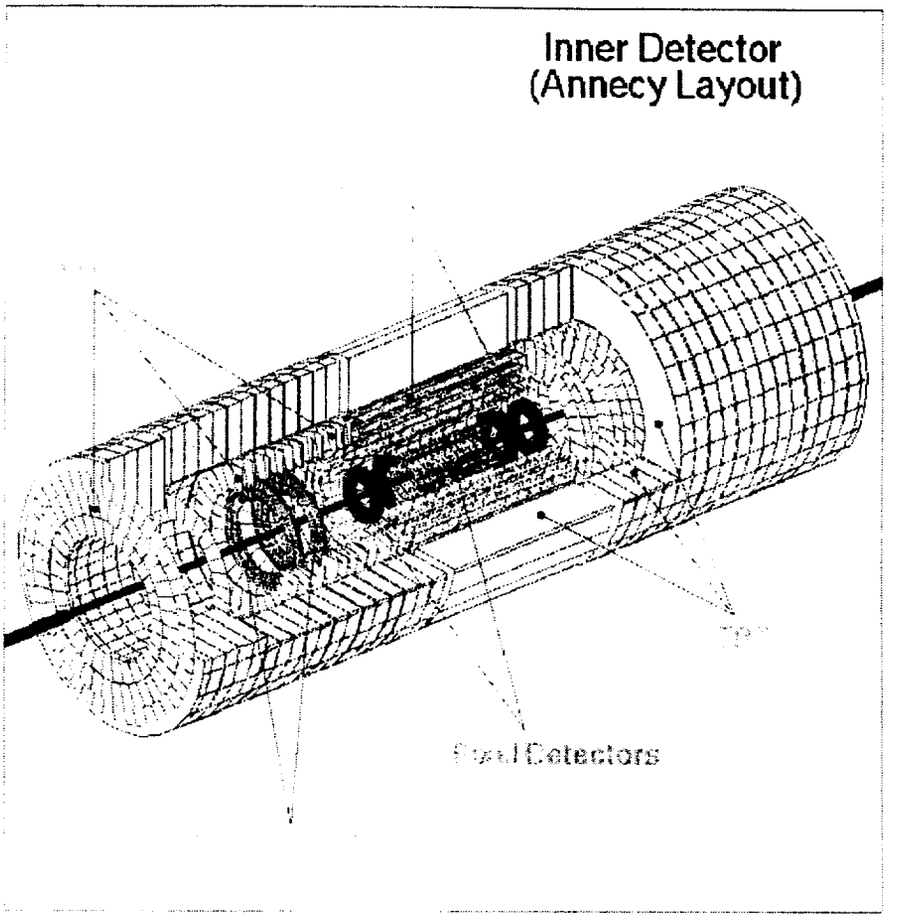

Figure 1: *Three-dimensional cutaway view of ATLAS Inner Detector.*

The ATLAS Inner Detector is defined by the boundaries of the barrel electromagnetic calorimeter cryostat, i.e. a radius R smaller than 115 cm (the tolerances for the cryostat are outside this value), and of the endcap electromagnetic cryostats and moderators, i.e. $|z| < 340$ cm. The endcap moderators are situated from $|z| = 340$ cm to 345 cm. There is no barrel moderator foreseen anymore in the present layout.

The beam pipe, 1 mm thick Beryllium (or equivalent) corresponding to 0.3% X_0 at normal incidence, has a diameter of ~ 5 cm. The details of the layout of the beam pipe and its supports/flanges/pumps over the full length of the inner cavity are not yet finalised.

The Inner Detector can be divided into three parts, both geometrically and mechanically: a barrel part and two endcap parts on each side. The barrel part

is characterised by active layers with a cylindrical geometry (barrel straw tracker or TRT, barrel silicon strip layers or SCT and barrel pixels or BPIX), with the exception of the endcap pixel disks (or EPIX), which are situated at small enough z to be integrated into the barrel mechanics. The endcap parts are characterised by active layers with a disk-like geometry (endcap straw tracker or TRT, micro-strip gas chambers or MSGC and Gallium Arsenide disks or GaAs).

The cylindrical layers measure accurately $R\phi$ and to a lesser extent z, whereas the disk layers measure accurately ϕ and to a lesser extent R. The vertexing and precision tracking layers are situated at the smaller radii, whereas the continuous straw tracker layers are situated at the larger radii. The only exception consists of the large radius MSGC wheels, one at each end of the cavity ($332 < |z| < 337$ cm) over $50 < R < 98$ cm. This layout of the Inner Detector is expected to give good momentum resolution, robust pattern recognition and electron identification over $|\eta| < 2.5$, as discussed in [1]. With the addition of a vertexing layer for the initial lower luminosity running, it is also expected to provide very accurate measurements of secondary vertices and of exclusive B-hadron final states, as described in [2].

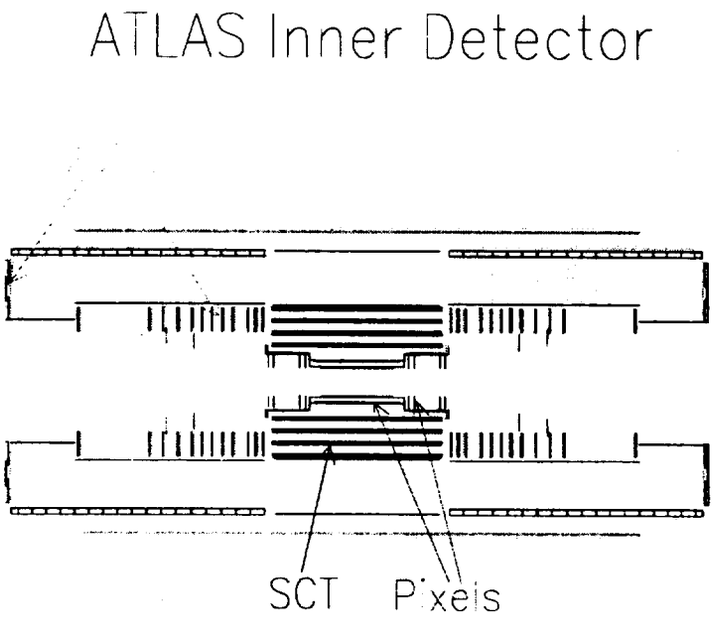

Figure 2: *Two-dimensional view in the $(R-z)$ plane of the ATLAS Inner Detector (no vertexing layer).*

Fig. 1 shows an exploded view of the Inner Detector in three dimensions. The various subdetector elements can better be seen in fig. 2, which shows them in the $(R-z)$ plane. The minimum radii of the semiconductor tracker elements have been chosen in terms of survival to radiation damage, as abundantly discussed elsewhere, whereas the minimal radii of the gaseous detectors have been chosen more in terms of occupancy.

As can be seen in fig. 2, the services and supports for the barrel tracker represent quite a large amount of space and (at least potentially) of material. These services and supports can better be seen in figs. 3 and 4, which show an enlarged view of the presently foreseen options for the low luminosity barrel trackers. Fig. 3 shows the silicon-strip option, a double-sided layer at 6 cm radius, of 23 cm half-length. Over its active area, this layer is expected to give a minimal amount of material ($\sim$ 0.5% X_0 for normal incidence). This however results in a much larger amount of material ($\sim$ 4-5% X_0) at the ends of this layer, depicted schematically as a box in the figure. Fig. 4 shows the pixel option, a layer at 4 cm radius, of 35 cm half-length (thus covering the full Inner Detector η-coverage) and consisting of the same pixels (50 $\times$ 300 μ) as the two pixel layers at larger radius. With its smaller radius but larger amount of material, this layer yields roughly the same performance in $R\phi$ impact parameter resolution as the strip layer [3].

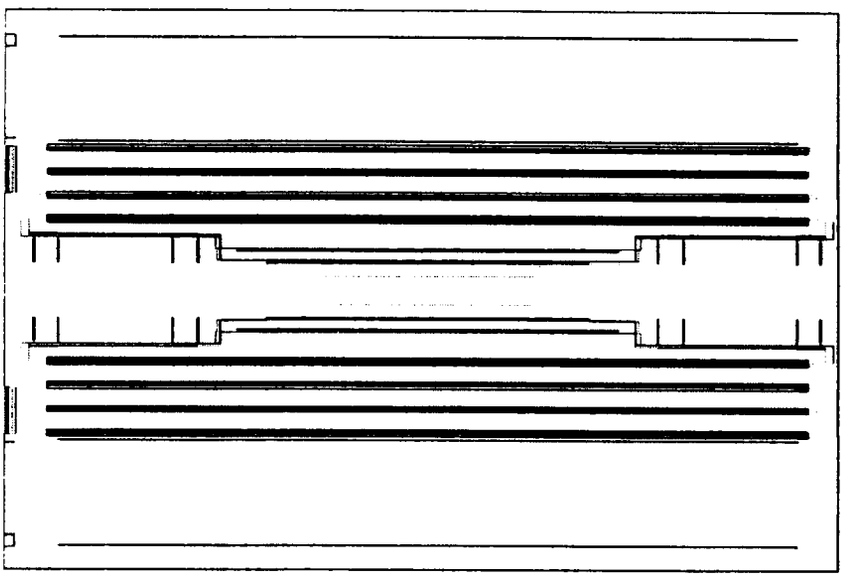

Figure 3: *Two-dimensional view in the $(R-z)$ plane of the barrel part of the ATLAS Inner Detector with the silicon strip vertexing layer at a radius of 6 cm.*

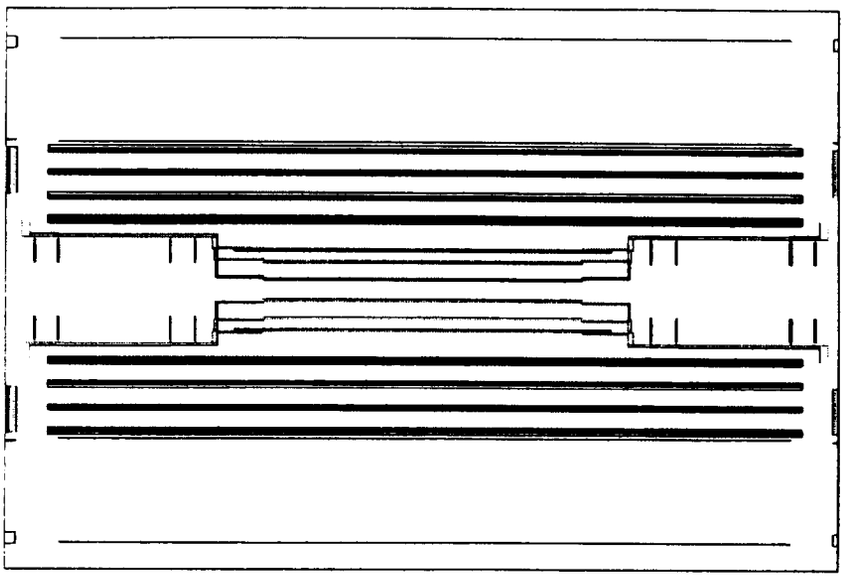

Figure 4: *Two-dimensional view in the (R−z) plane of the barrel part of the ATLAS Inner Detector with the pixel vertexing layer at a radius of 4 cm.*

In DICE the possible options for the inner tracker geometry (INNE) are thus the following:

- GEOM 3, for high luminosity studies (no vertexing layer);
- GEOM 4, with the double-sided strip layer at R = 6 cm;
- GEOM 5, with the pixel layer at R = 4 cm.

2 Subdetector geometries

Here we briefly describe the various subdetector geometries as they have been implemented in DICE. For several of the subdetectors (e.g. for the SCT and the pixels), detailed notes describing the geometry and mechanics/electronics layout are in preparation. The geometry implemented in DICE is to a large (but not full) extent faithful to the present understanding of how the subdetectors could be built.

The main geometrical features of each subdetector are summarised below, together with the number of electronics channels and the area of the active detector elements. These areas do not in general correspond exactly to that used for CORE costings, where yield, wastage and spares are taken into account.

2.1 Pixels

The pixel detectors consist of two cylindrical barrel layers, situated at radii of 11.5 and 16.5 cm, and of eight endcap disks (four on each side) at z-positions

of 49.92, 55.40, 79.90 and 85.00 cm. An additional cylindrical pixel layer at a radius of 4 cm is considered for the initial low-luminosity running. The cylindrical layers at 4 cm and 11.5 cm radius have an active half-length of 35.04 cm, and the one at 16.5 cm radius has an active half-length of 45.42 cm. The endcap disks all cover radii between 11.45 cm and 21.25 cm. The presently foreseen pixel size is 50 μ $\times$ 300 μ in $R\phi$ $\times$ z and the thickness of silicon is 150 μ.

The barrel layers consist of 16, 45 and 65 ladders respectively as radius increases. The ladders are tilted by corresponding angles of 11.5°, 9.98° and 9.74°. This ensures an overlap between neighbouring ladders of 5.2, 1.3 and 1.4 mm respectively, corresponding roughly to 6 active pixel rows.

The active pixel areas are 1.38 m^2 for the barrel and 0.79 m^2 for the endcaps, with a possible additional 0.18 m^2 for the 4 cm radius layer. The number of pixels is 8.2 10^7 for the barrel and 5.2 10^7 for the endcaps, with a possible additional 1.1 10^7 for the 4 cm radius layer. More details can be found in [4].

The barrel and endcap pixels are activated in DICE as detectors BPIX and EPIX. The size of the pixels and of the dead areas between detectors in z can be changed at the digitisation stage (i.e. after GEANT simulation) using the DETD datacard. There is no detailed simulation of the charge deposition in the pixels nor of the front-end electronics in the present code.

2.2 Barrel silicon strips

The barrel silicon strip subdetector consists of four cylindrical layers at radii of 30, 40, 50 and 60 cm, with an active half-length of 82.05 cm. The active silicon thickness is 300 μ. Each layer consists of ladders (or skis), positioned with tilt angles of 7, 6, 5 and 5° respectively as radius increases. The geometry is presently based on single-sided 75 μ pitch modules, of 6 cm width and 12 cm length, containing two detectors bonded together in z. Each layer consists of 14 modules, containing each four such detectors grouped into back-to-back pairs. One pair measures directly $R\phi$, whereas the other one is tilted by a small stereo angle (set by default to 40 mrad), so as to measure z. This stereo angle has unfortunately to be changed in the geometry, i.e. before GEANT simulation, if one wishes to study other geometries. In particular, an option with crossed strips is available.

The total area of active silicon is $\sim$ 41 m^2, corresponding to a total of 4.4 10^6 electronics channels in the case of a direct readout of all strips. More details can be found in [5].

The barrel silicon strip detectors can be activated in DICE as detector SCT. The strip pitch can be changed at the digitisation stage (i.e. after GEANT simulation). There is no detailed simulation of the charge deposition in the silicon, nor of the front-end electronics in the present code.

An extra layer of silicon strips, with a double-sided structure can be activated as detector SITV if one selects GEOM 4 for detector INNE (see above). This layer is at a radius of 6 cm and has a half-length of 23.04 cm. The strips measuring $R\phi$

have a 35 μ pitch in the simulation, thus yielding an accuracy of 10 μ. Their length is 23.04 cm, which allows for a minimum-material layer design without any electronics on the detector itself (as in most of the present experiments). The z-measurement is performed with crossed strips of 70 μ pitch in the simulation. More details can be found in [7].

2.3 Endcap precision tracking

The layout of the endcap precision tracking was obtained by requiring that all tracks from the primary vertex cross six precision layers. Two of these are the barrel or endcap pixel layers and the other four are a combination of barrel SCT, MSGC and GaAs. The GaAs disks supplement the MSGC disks, which have been constrained to provide measurements above a radius of 40 cm, at the largest rapidities. This 40 cm minimum radius for the MSGC should obviously not be taken as a number cast in stone. Details on the optimisation of the endcap precision tracking layout and its connection to the precision barrel tracker layout can be found in [9].

2.3.1 Microstrip gas chambers or MSGC

The MSGC consist of a set of 12 small wheels (spanning active radii between 44 and 60 cm) and one large wheel (spanning an active radius between 50 and 96 cm) for each endcap part.

Each small wheel is 5 cm thick along z and consists of 30 tiles, each containing 3 sets of 512 measurement strips. The strips all have 16 cm active length along radius and $\sim$ 180 μ pitch. The strips are arranged in a keystone pattern, i.e. the strip pitch increases with radius. One set of strips measures ϕ, i.e. all strips point to the transverse vertex. The other two sets of tiles are rotated by $\pm$ 1^o with respect to the first one and thus measure the so-called u-v coordinates from which the radius R can be extracted. The z-positions of the centres of the 12 small wheels are at 90.0, 97.2, 104.3, 118.7, 128.5, 138.2, 148.0, 157.7, 171.1, 184.5, 197.8 and 265.6 cm.

Each large wheel is also 5 cm thick along z and consists of 3 concentric rings of 16 cm tiles. The first ring is at z = 333.0 cm and at a radius between 50 and 66 cm, the second ring is at z = 336.0 cm and at a radius between 66 and 82 cm, and the third ring is at z = 333.0 cm and at a radius between 80 and 96 cm. Their respective strip pitches are 190, 201 and 212 μ. The positions of the cracks between tiles of each type are offset in ϕ with respect to one other. In addition each wheel is rotated in ϕ with respect to the previous one.

The total area of active MSGC counters is 37.6 m^2 for the small wheels and 13.2 m^2 for the large wheels. This corresponds to 1.11 10^6 electronics channels for the small wheels and to 0.36 10^6 electronics channels for the large wheels.

The MSGC detectors can be activated in DICE as detector MSGC. The details of ionisation in the gas, electron drift, diffusion and gas gain fluctuations are included in the simulation. This, together with a simple model of the front-end electronics,

in terms of a discriminator threshold and a noise level, determines the detector efficiency and position resolution. The gas is assumed to be Ar/DME (50:50), which has a drift velocity of 50 μ/ns at the operating voltages. The gas gap is 2.2 mm and charge will therefore be collected over 2 successive bunch crossings; however, currently in DICE, all charge is assumed to originate from the centre of the gas gap.

2.3.2 GaAs disks or Forward SCT

The GaAs detector consists of two wheels at z = 155.7 and 182.5 cm in each endcap part. Each wheel consists of two rings of back-to-back single-sided GaAs strip counters. Each counter contains 460 strips of 50 μ pitch and 7.7 cm active length. The strips are parallel and each counter is rotated by $\pm$ 1°, so that each ring provides a (u-v) measurement. The first wheel covers radii between 25 and 40 cm, whereas the second one covers radii between 29 and 44 cm. The thickness chosen for the GaAs substrate is 200 μ.

The total area of active GaAs is $\sim$ 2.8 m^2 for a total of about 800000 electronics channels. The GaAs wheels can be activated in DICE as detector GAAS. The strip pitches and stereo angles can be changed at the digitisation stage (i.e. after GEANT simulation). There is no detailed simulation of the charge deposition in the GaAs nor of the front-end electronics in the present code.

2.4 Transition radiation straw tracker or TRT

The TRT consists of three distinct parts, a barrel part consisting of a cylindrical structure containing axial straws embedded in a polypropylene foam, and two endcap parts consisting of 18 wheels on each side, equipped with radial straw layers interleaved with polypropylene foils. The straws have an inner diameter of precisely 4 mm and a wall thickness of $\sim$ 85 μ.

The barrel TRT consists of 64 concentric layers of 160 cm long axial straws. The radial distance between successive layers is 6.8 mm. In a given layer the straws are also spaced by $\sim$ 6.8 mm, and each layer is offset in ϕ by a fraction of this distance with respect to the previous one. With this geometry, an average of 36 crossed straws are expected for all tracks with $p_T > 1$ GeV [8]. At z = 0, all the wires inside the straws are interrupted and each side is read out independently. The barrel TRT thus comprises 50124 straws and 100248 electronics channels. Its active volume covers radii between 63.0 and 107.2 cm. The spaces between straws are filled with a low-density polypropylene foam, which produces transition radiation X-rays.

The endcap TRT modules (18 on each side) have a length of 13.4 cm (except the last one which is 7 cm long) along z, and are of 3 different types:
• the first 6 modules, at z = 89.0, 102.6, 116.1, 130.5, 144.9, and 159.3 cm, consist of 16 layers of 768 straws. The straw active radius is between 64 and 103 cm. The distance between two successive layers is 8 mm along z and the free space is filled with 12 foils of polypropylene foil radiator;

• the next 7 modules, at z = 173.7, 187.2, 201.6, 215.1, 228.6, 242.1, and 255.6 cm, consist of only 8 layers of 768 straws, with the same straw radial dimensions. The distance between two successive layers is 16 mm along z and the free space is filled again with 12 foils of polypropylene foil radiator. These wheels therefore have half the density of the first ones, and thus minimise the amount of material;
• the last 4 full-length wheels, at z = 270.0, 283.5, 297.0, and 310.5 cm, consist of 16 layers of 608 straws. The last shorter wheel, at z = 324.0 cm, consists of 8 layers of 608 straws. The straw active radius is between 50 and 103 cm. This maximizes the rapidity coverage of the TRT.

There are thus a total of 321024 straws in the endcap TRT, leading to a total number of 421272 electronics channels and 300 km of wire. The TRT can be activated in DICE as detector XTRD. The ionisation losses in the straws are simulated in detail (except for Lorentz angle effects) for a nominal gas gain of 2.5 10^4. The default gas mixture used is 70% Xe + 20% CF_4 + 10% CO_2. The transition radiation (TR) photons are generated as a global spectrum transported along the electron trajectory with the appropriate production probabilities, absorption losses and probability of observation in the sensitive gas. The absolute TR-fluxes are tuned to reproduce test-beam data. The digitisation stage simulates as accurately as possible the front-end electronics response.

3 Accuracies and momentum resolution

A separate note [9] describes in some detail the expected momentum resolution for this layout, including the effect of the non-uniformity of the magnetic field. Here we only summarise the expected individual sub-detector resolutions:
• the pixel resolution is 50 $\mu/\sqrt{12}$ in Rϕ and 300 $\mu/\sqrt{12}$ in z;
• the silicon strip resolution is 75 $\mu/\sqrt{12}$ per Rϕ measurement, corresponding to $\sim$ 15 μ per layer. The z-resolution is $\sim$ 540 μ for the chosen 40 mrad stereo angle;
• the MSGC resolution is 45 μ per Rϕ measurement, corresponding to $\sim$ 35 μ per wheel with a (ϕ, u, v) measurement. The resolution in R is $\sim$ 3.3 mm per u or v measurement, corresponding to $\sim$ 2.3 mm per wheel;
• the GaAs resolution is 50 $\mu/\sqrt{12}$ per Rϕ measurement, corresponding to $\sim$ 10 μ per disk. The resolution in R is $\sim$ 0.8 mm per u or v measurement, corresponding to $\sim$ 0.6 mm per disk;
• the TRT single straw resolution is 170 μ at low luminosity from the drift-time measurement. This increases to 210 to 220 μ at the highest LHC luminosities, albeit with much reduced efficiency.

The numbers above only reflect the intrinsic accuracy of the proposed sub-detectors. Alignment errors will have to be included in future studies, when a concerted effort will be made to evaluate the tracker alignment strategy with real tracks.

The impact parameter resolution of the inner tracker and its various vertexing

options has been evaluated, using a well-proven analytical technique [3], both in the Rϕ-plane and in the longitudinal direction.

4 Material distributions, supports and services

4.1 Global numbers and plots

In order to obtain a realistic evaluation of the material in the inner tracker, the description of the sub-detectors includes, within the limits of present knowledge, mechanical supports, electronics, and services. In most cases, these are described using simplified geometries (e.g. averaging over ϕ). The total material thicknesses are expected however to represent as faithfully and as realistically as possible the present understanding of the inner tracker design. The MSGC and GaAs services, which represent a very small amount of material per disk, have not been described in the present geometry except at large radius. A 2 cm thick cylinder, at a radius between 111 and 113 cm and for $84 < z < 340$ cm, corresponding to approximately 2% X_0 at normal incidence, describes schematically the barrel services. In a similar way, at a smaller radius between 109.5 and 111 cm, a cylinder with varying thickness (from 0.5 cm for $89 < z < 170$ cm to 1.5 cm for $250 < z < 340$ cm) describes schematically the endcap services.

Table 1: *Amount of material in % X_0 of the various sub-detectors, for different values of η.*

Sub-detector	$\eta = 0.0$	$\eta = 1.0$	$\eta = 1.3$	$\eta = 1.8$	$\eta = 2.3$
Barrel pixels	2.3	3.5	4.2	8.7	-
Endcap pixels	-	-	-	4.4	1.8
Silicon strips	6.5	18.9	15.9	7.6	1.8
Gallium arsenide	-	-	-	-	5.0
MSGC	-	-	7.7	13.3	6.0
Straw tracker	9.7	26.1	27.8	37.4	11.6
Total material	18.5	48.5	55.6	71.4	26.2

Table 1 shows, at η =0.0, 1.0, 1.3, 1.8 and 2.3, the total amount of material (integrated up to a radius of 115 cm), separately for each sub-detector and also for the whole inner tracker. The total material varies between a minimum of 18.5% X_0 at η = 0.0 to a maximum of $\sim$ 70% X_0 for 1.7 < η < 1.8. The straw tracker with its radiator and supports represents about 50% of the total material over the full rapidity coverage. Table 1 illustrates how the contributions from the various precision tracking elements vary as a function of η.

A considerable fraction of the material is concentrated at large radius, as illustrated in fig. 5, which shows that for a radius smaller than 103 cm, i.e. after disregarding essentially only some supports (endcap TRT wheels) and services, the total material of the tracker is always below the target figure of 50% X_0. On the other hand, for η $\sim$ 1.5, almost 30% X_0 of tracker material is concentrated at rather small radius (R < 63 cm). The impact of this amount of tracker material on the electromagnetic calorimeter performance has been shown to produce significant tails in the reconstructed energy distributions of electrons with transverse energies below $\sim$ 40 GeV [10]

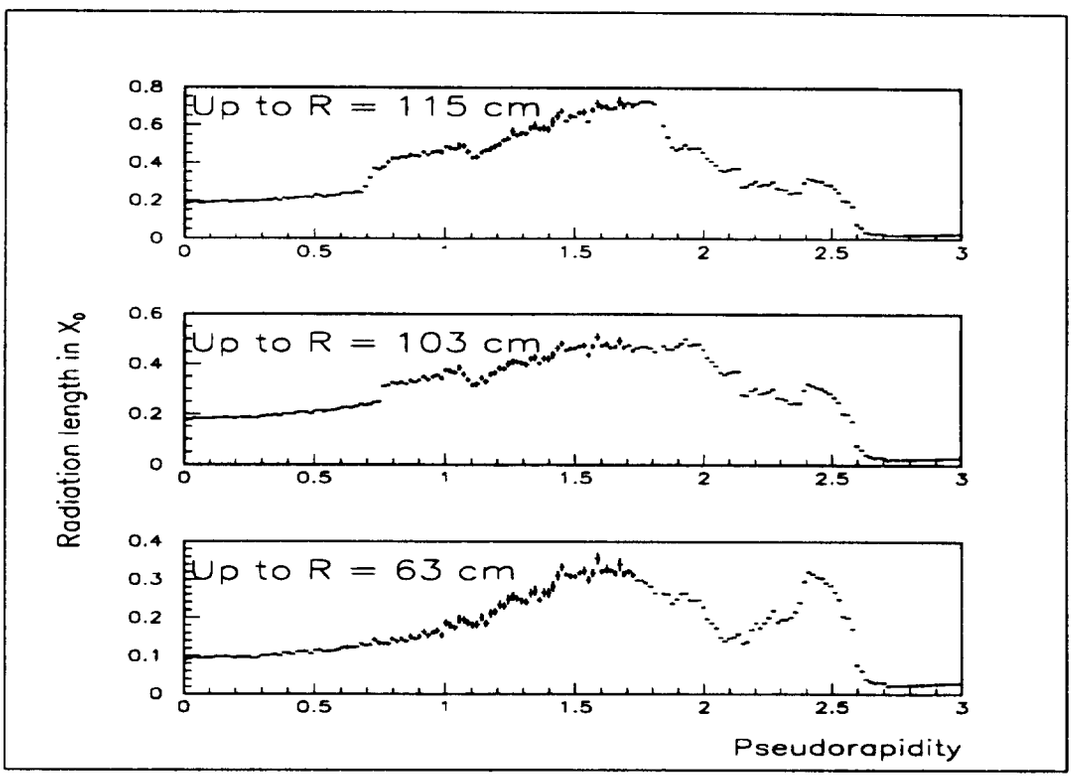

Figure 5: *Amount of material in X_0 versus pseudorapidity for complete high luminosity inner tracker layout (top), for material at radius smaller than 103 cm (middle), and for material at radius smaller than 63 cm (bottom).*

Figures 6 to 14 show the integral distributions of material in the tracker as a function of radius, for η-values increasing from 0.0 to 2.5. The histogram bins are filled only when crossing detector material and these figures thus illustrate where the bulk of the tracker material is concentrated as radius increases. The spikes in some histograms are spurious, i.e. only reflect a binning problem in that particular histogram. Although it is not expected that the material in the tracker volume at radii below $\sim$ 100 cm will increase in the future, and although every effort is being pursued to decrease the overall tracker material budget, it is clear that these numbers are far from being final. More details on each sub-detector can be found at the end of this note.

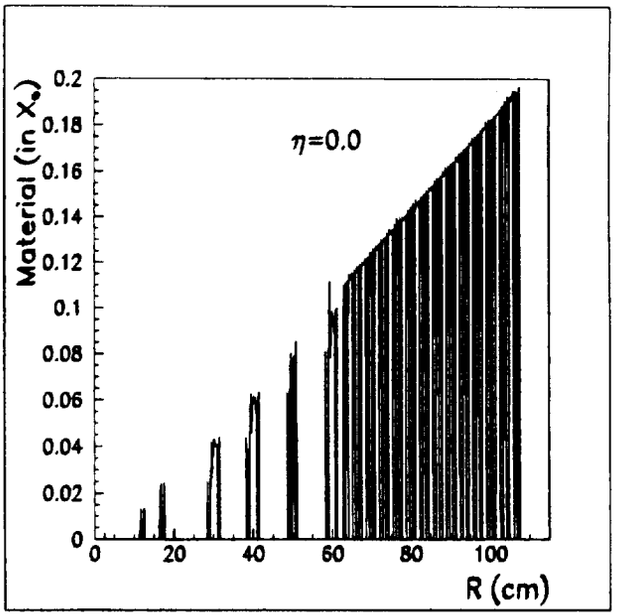

Figure 6: *Integral amount of material in X_0 versus radius, at η =0.0, for the high luminosity inner tracker layout. The histogram bins are filled only if they contain material which is not air or vacuum.*

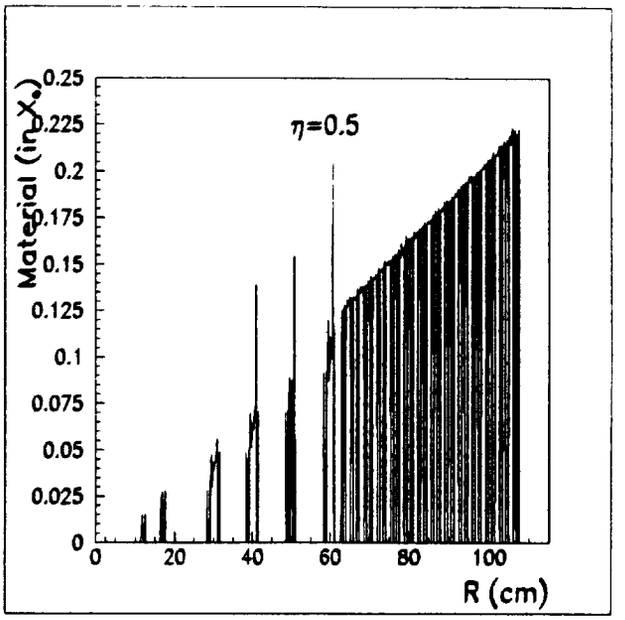

Figure 7: *Integral amount of material in X_0 versus radius, at η =0.5, for the high luminosity inner tracker layout. The histogram bins are filled only if they contain material which is not air or vacuum.*

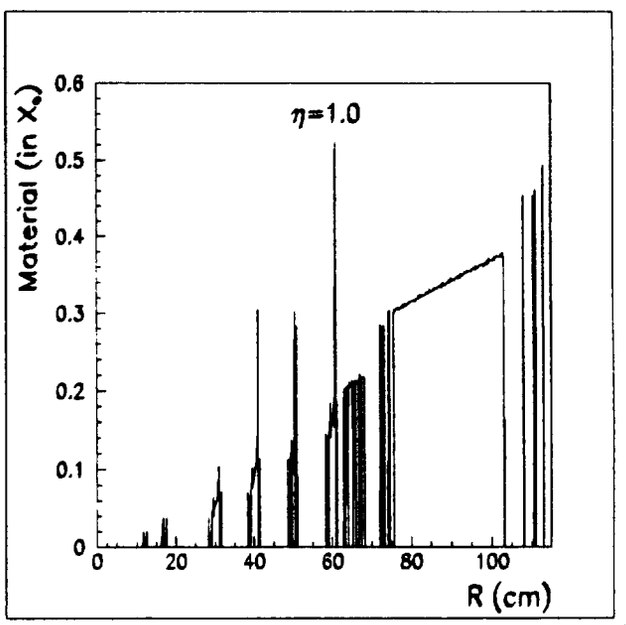

Figure 8: *Integral amount of material in X_0 versus radius, at η =1.0, for the high luminosity inner tracker layout. The histogram bins are filled only if they contain material which is not air or vacuum.*

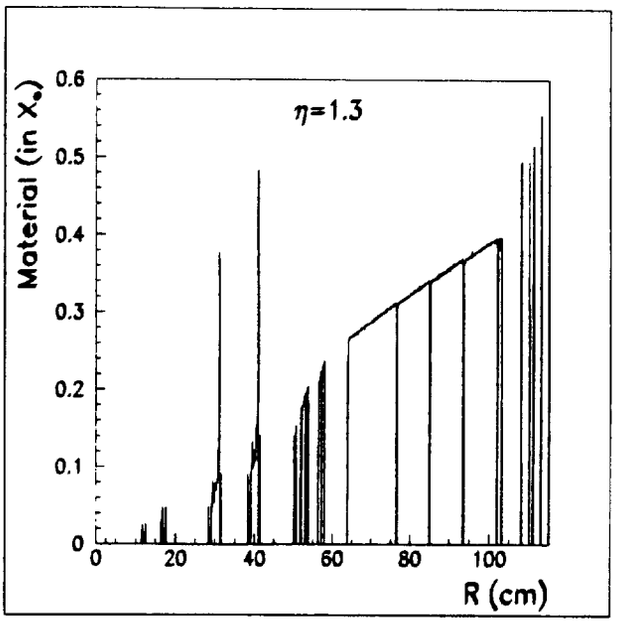

Figure 9: *Integral amount of material in X_0 versus radius, at η =1.3, for the high luminosity inner tracker layout. The histogram bins are filled only if they contain material which is not air or vacuum.*

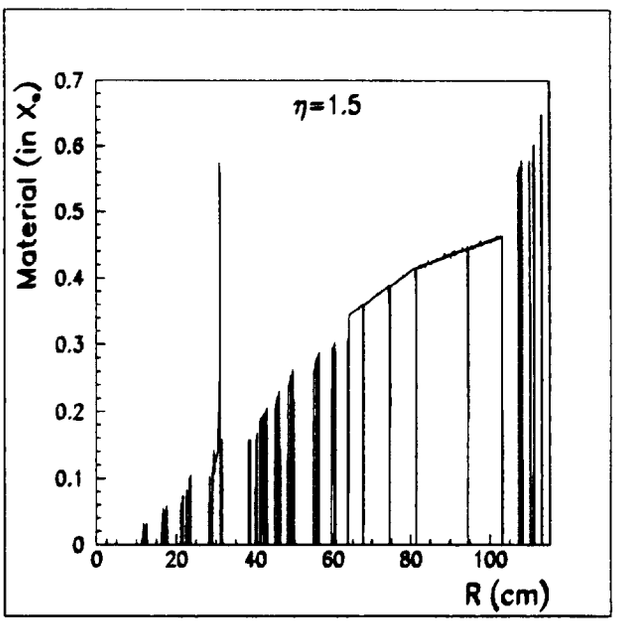

Figure 10: *Integral amount of material in X_0 versus radius, at η =1.5, for the high luminosity inner tracker layout. The histogram bins are filled only if they contain material which is not air or vacuum.*

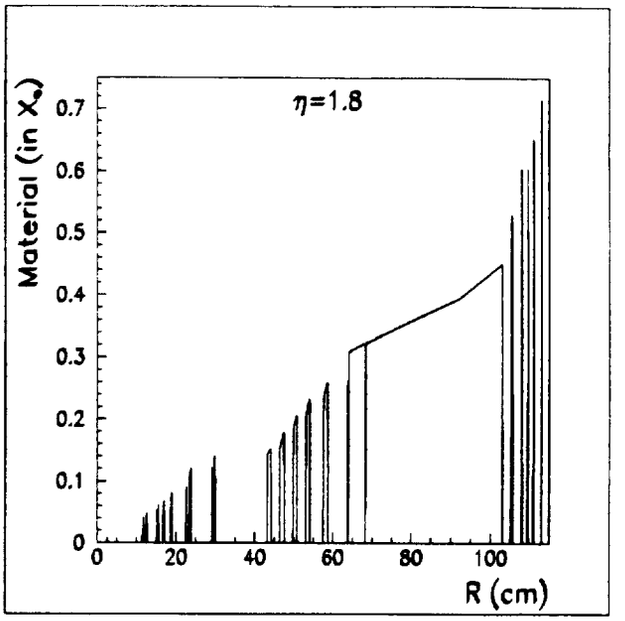

Figure 11: *Integral amount of material in X_0 versus radius, at η =1.8, for the high luminosity inner tracker layout. The histogram bins are filled only if they contain material which is not air or vacuum.*

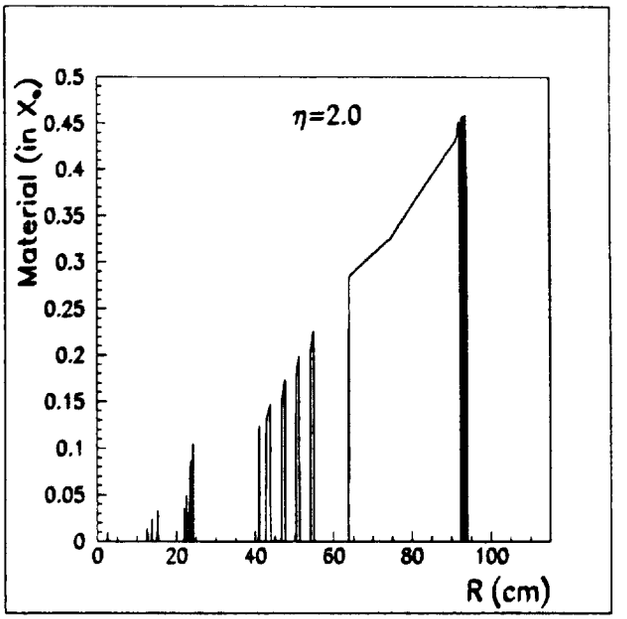

Figure 12: *Integral amount of material in X_0 versus radius, at η =2.0, for the high luminosity inner tracker layout. The histogram bins are filled only if they contain material which is not air or vacuum.*

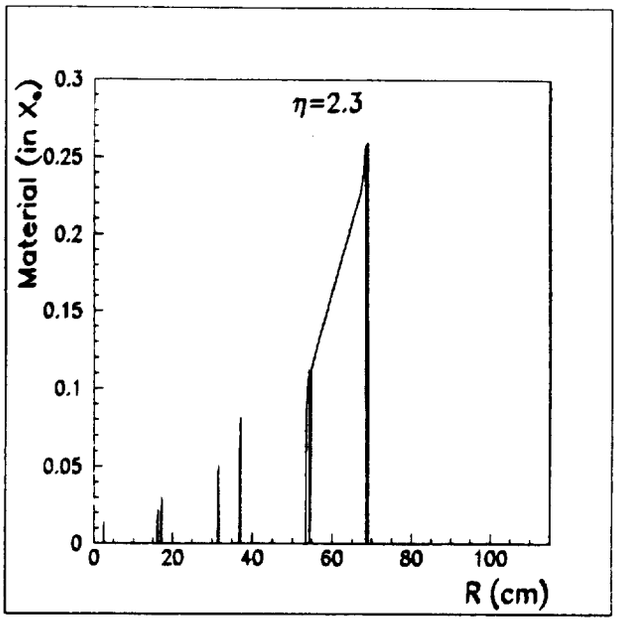

Figure 13: *Integral amount of material in X_0 versus radius, at η =2.3, for the high luminosity inner tracker layout. The histogram bins are filled only if they contain material which is not air or vacuum.*

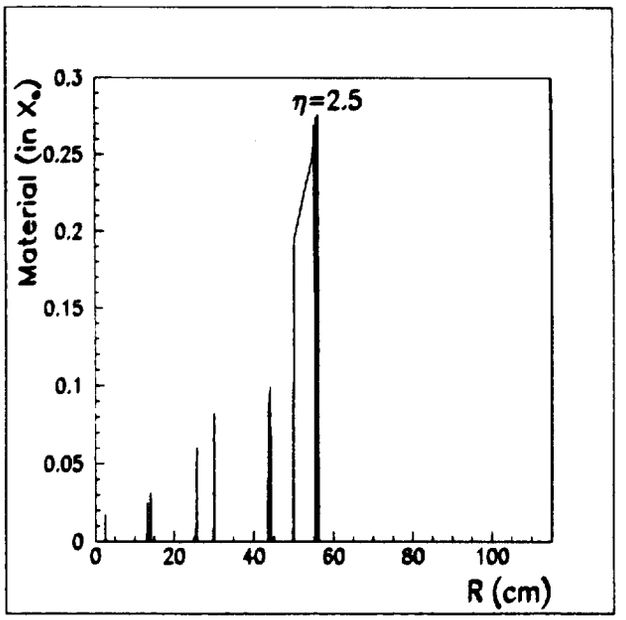

Figure 14: *Integral amount of material in X_0 versus radius, at η =2.5, for the high luminosity inner tracker layout. The histogram bins are filled only if they contain material which is not air or vacuum.*

4.2 Pixels and barrel SCT

Fig. 15 shows the distribution of material in the silicon strip detector and the barrel/endcap pixel detectors. These plots include all the supports/services specific to the pixels and to the silicon strip ladders. Not included are the services at z $\sim$ 80 cm nor the overall support structure for the barrel precision tracker. Fig. 16 shows, for the high luminosity barrel precision tracker, the total amount of material versus pseudorapidity, without (top) and with (bottom) these services/supports. The services are included up to the crack between the barrel and endcap electromagnetic calorimeters.

Each pixel layer amounts to $\sim$ 1.1% X_0, at normal incidence, to which the substrate contributes about 0.16% X_0. Each silicon strip layer amounts to $\sim$ 1.6% X_0, at normal incidence, to which the substrate contributes about 0.64% X_0.

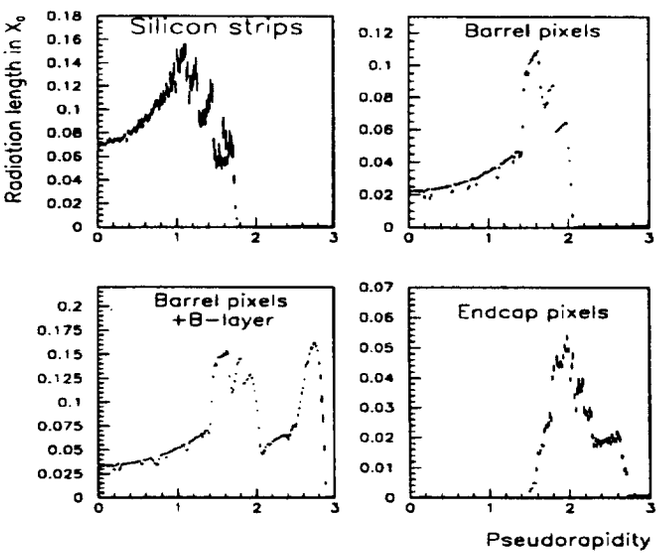

Figure 15: *Amount of material versus pseudorapidity for the silicon strips (top left), the barrel pixels (top right), the barrel pixels with the vertexing pixel layer (bottom left), and the endcap pixels (bottom right).*

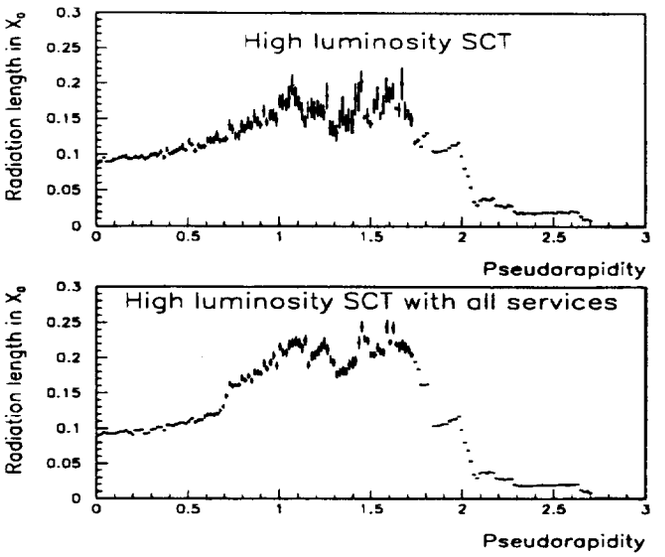

Figure 16: *Amount of material versus pseudorapidity for the high luminosity barrel precision tracker, without (top) and with (bottom) the services/supports at* $z \sim 80$ *cm.*

4.3 Endcap precision tracking

Figure 17 shows the amount of material versus pseudorapidity for the MSGC (top) and GaAs (bottom) detectors. Each MSGC wheel amounts to $\sim 3.4\%$ X_0, at normal incidence, to which the substrate (presently heavy glass) contributes about 1.7% X_0. Each GaAs wheel amounts to $\sim 2.5\%$ X_0, at normal incidence, to which the substrate contributes about 1.7% X_0.

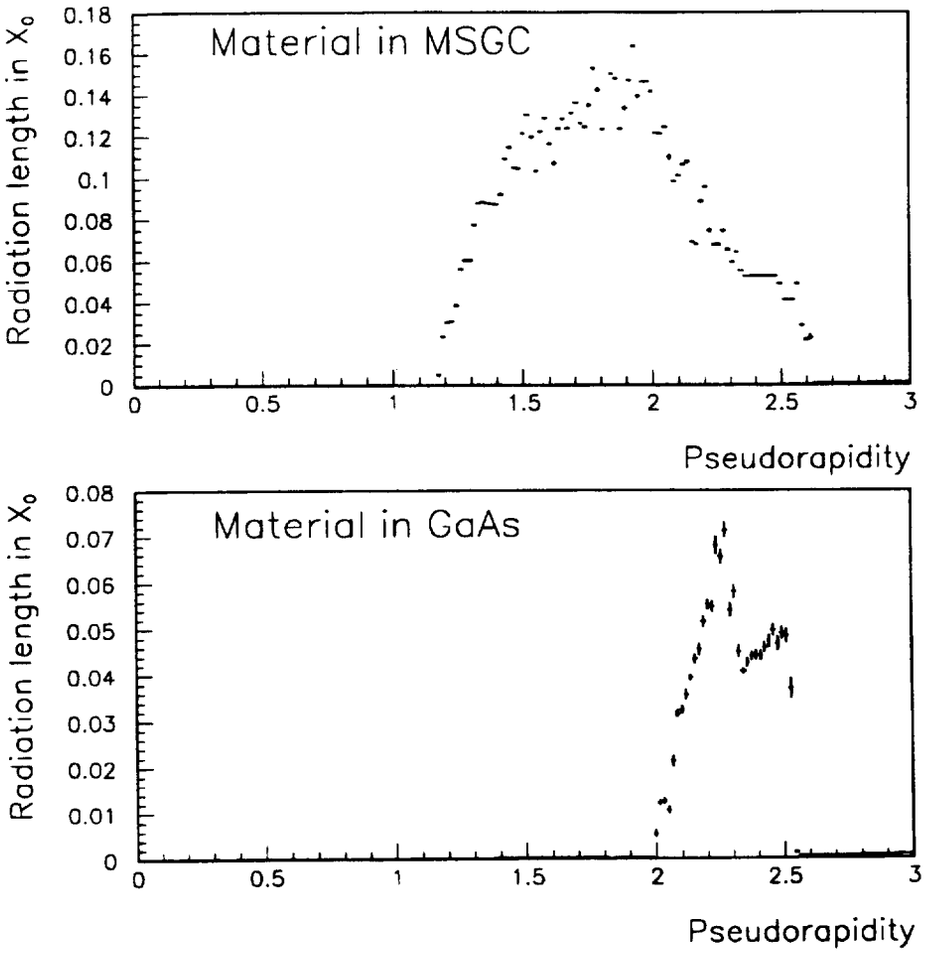

Figure 17: *Amount of material versus pseudorapidity for the endcap precision tracker, separately for the MSGC (top) and for the GaAs (bottom).*

4.4 Straw tracker

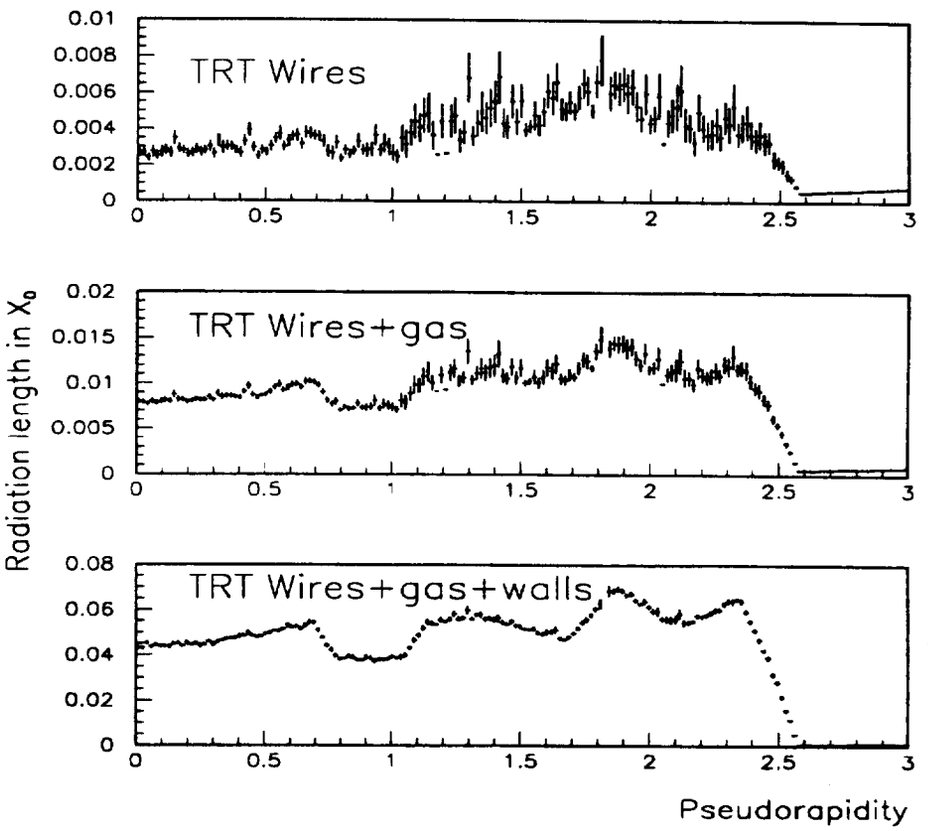

Figure 18: *Amount of material versus pseudorapidity for the TRT straws, including successively the wires (top), the wires and the gas (middle), and the wires, the gas and the straw walls (bottom).*

Figure 18 shows the amount of material versus pseudorapidity for various ingredients of the straws. The straw walls (including the C-fibre reinforcements) contribute most of the straw material, i.e. $\sim$ 80%. The total amount of material due to the straws themselves varies between 4% and 7% X_0 over the pseudorapidity coverage. If one includes the radiator material, as shown in fig. 19, the material is approximately doubled, ranging from 8% to 17% X_0. Figure 19 also shows that the outer endcap wheels, with their electronics and services, contribute a large amount of material, $\sim$ 16% X_0, at $\eta = 1.8$, although they will be built of very light materials (5% X_0 at normal incidence). The bottom part of fig. 19 includes, in addition to the barrel support cylinders and endcap wheel supports, the barrel end-flanges and electronics (6% X_0 at normal incidence) and all the TRT services.

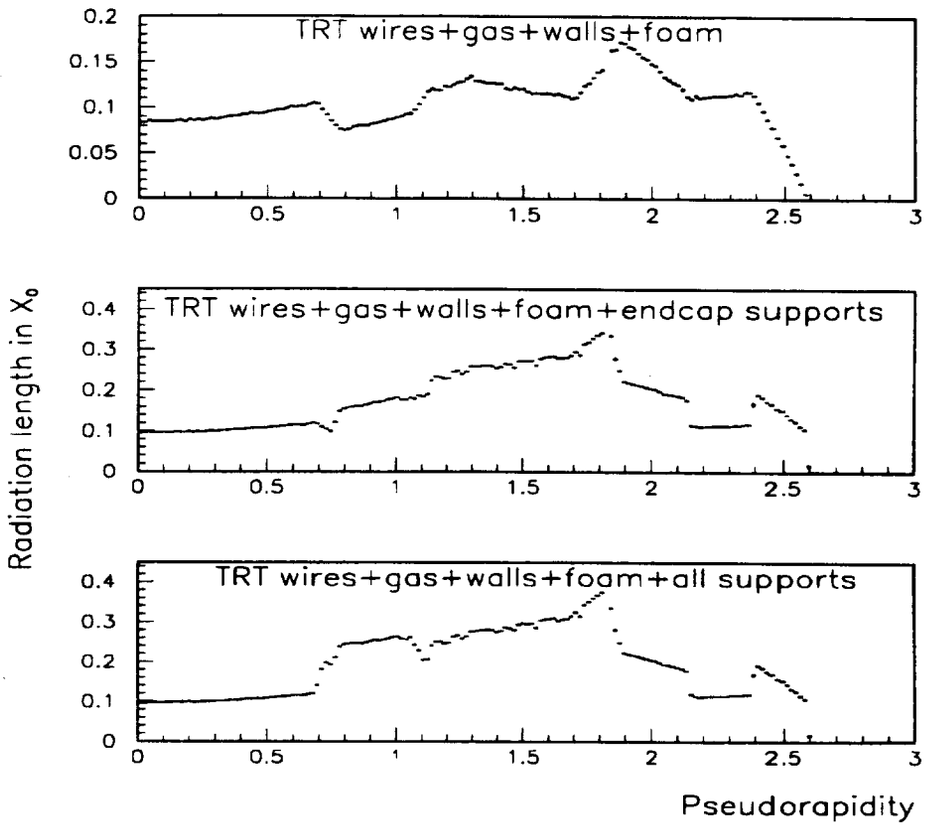

Figure 19: *Amount of material versus pseudorapidity for the TRT, including successively the straws and the foam (top), the straws, the foam and the endcap supports (middle), and the straws, the foam, the endcap supports and the barrel flanges/services (bottom).*

5 Conclusions

The ATLAS Inner Tracker layout, as agreed upon during the September ATLAS week, is described in detail in DICE using GEANT. This layout, although certainly not final, is believed to meet the performance specifications, in terms of momentum resolution, pattern recognition, vertexing and particle identification. It also reflects as faithfully as possible the present understanding of the engineering of the tracker. The next step (most probably post-Technical Proposal) will be to adapt the various track reconstruction packages to this new layout.

References

[1] D. Froidevaux and M.A. Parker, ATLAS Internal Note, INDET-NO-046.

[2] ATLAS Collaboration, "B physics with the ATLAS experiment at LHC", CERN/LHCC/93-53, 15 October 1993.

[3] S. Gadomski, BPHY-TR-043.

[4] D. Bintinger et al., ATLAS Internal Note, to be published.

[5] A. Reichold and SCT group, ATLAS Internal Note, to be published.

[6] S. Gadomski et al., ATLAS Internal Note, INDET-NO-035.

[7] A. Poppleton et al., ATLAS Internal Note, to be published.

[8] P. Nevski, RD6 Internal Note 39.

[9] A. Poppleton et al., ATLAS Internal Note, to be published.

[10] F. Gianotti and B. Mansoulie, PHY-TR-167.